

Removing Multi-frame Gaussian Noise by Combining Patch-based Filters with Optical Flow

Kireeti Bodduna^{1,2} and Joachim Weickert¹

Abstract—Patch-based methods such as 3D block matching (BM3D) and the non-local Bayes (NLB) approach produce state-of-the-art results for removing Gaussian noise from single-frame images. In this work, we propose two extensions for these filters when there exist multiple frames of the same scene. To this end, we combine two novel inter-frame connectivity strategies with robust optical flow methods. Our extensions do not require additional parameters and outperform existing techniques qualitatively by a significant margin. By exploiting spatial and temporal separability, one of our approaches is also faster than its competitors. Since our strategy is not restricted to BM3D and NLB, it can be generalised to other similar single-frame patch-based methods.

Index Terms—patch-based methods, multi-frame denoising, image sequence denoising, video denoising, Gaussian noise.

I. INTRODUCTION

Restoring images corrupted with various types of noise degradations is a classical image processing problem [1]–[9]. Additive white Gaussian noise (AWGN), Poissonian and Poissonian-Gaussian mixture noise types are the most studied models in this application. AWGN elimination methods are particularly important because they can be combined with variance stabilising transformations [10]–[12] for also removing the latter two types of noise.

In the single-frame AWGN elimination scenario [13]–[24], BM3D [21], [22] and NLB [18], [19] produce the best results. Both of them are non-local patch-based methods which utilise the similar information available at distant regions in the image. BM3D in particular is used for comparative evaluation in articles that involve neural network-based methods [25] or traditional methods [18]. Both filters use a sequential strategy of grouping, collaborative filtering and aggregation. While grouping brings similar patches together to exploit the advantage of having more signal, collaborative filtering is responsible for simultaneous and efficient removal of noise at different pixels. The aggregation stage is a non-linear averaging technique that yields the final denoised image.

Multi-frame filters [26]–[42], on the other hand, utilise information from multiple frames of the same scene to compute the final denoised image. In this work, we concentrate on the fundamental problem of finding general approaches that can optimally extend single-frame patch-based methods such as NLB and BM3D to the multi-frame scenario.

There already exist two types of extensions [35]–[39] for BM3D and NLB. The first strategy exploits the advantage of having an extra degree of freedom by employing a separable spatio-temporal similarity-based grouping on a single reference frame [35], [36]. The other strategy makes use of the complete available information in all frames by employing combined spatio-temporal approaches [37]–[39]. We abbreviate these extensions as SF (single reference frame filtering) and CF (combined filtering), respectively. However, methods which combine the advantages of both these strategies and those which separately filter information in the spatial and temporal dimensions, have not been studied. A careful and systematic evaluation of these techniques is also missing.

Our Contribution. In order to address the above problem, in our recent conference paper [43] we introduced two types of extensions: Firstly, we combined the advantages of both the above existing extensions into a single method MF (multiple reference frame filtering) by employing a separable similarity measure on every frame. Secondly, we introduced two other extensions which utilise the advantage of separately filtering the different types of data in the temporal and the spatial dimensions. In the first strategy FA (filter-then-average), we performed the spatial filtering before the temporal averaging, while in AF (average-then-filter) we reversed this order. A comparative analysis of AF, FA, SF and MF when applied to BM3D on perfectly registered data, revealed that our proposed extension outperforms others.

In the present work we additionally make three novel contributions: Firstly, we also consider non-registered data. In contrast to [43], we combine our multi-frame filters with robust optical flow methods for dealing with the inter-frame motion. In contrast to other works, we juxtapose the performance simultaneously for registered and for non-registered data. This provides valuable additional insights into the influence of motion estimation errors on the filter performance.

Secondly, we provide the first comprehensive evaluation of general strategies how to extend single-frame filters to multi-frame ones. We apply all our extensions not only to BM3D (as in [43]), but also to NLB.

Last but not least, we propose better parameter selection strategies than in our conference paper. We shall see that this will even change the order in our experimental rankings. For the sake of completeness, we also include the extension CF that was missing in the evaluation of [43]. It represents the present state-of-the-art standard.

Paper Structure. In Section II we first review the central ideas behind the design of NLB and BM3D filters. We then introduce the five multi-frame extensions including our

¹Mathematical Image Analysis Group, Faculty of Mathematics and Computer Science, Saarland University, 66041 Saarbrücken, Germany.

²Electron Microscopy Group, Institute of Biophysics, Johann Wolfgang Goethe University Frankfurt, 60438 Frankfurt am Main, Germany.
email: {bodduna,weickert}@mia.uni-saarland.de

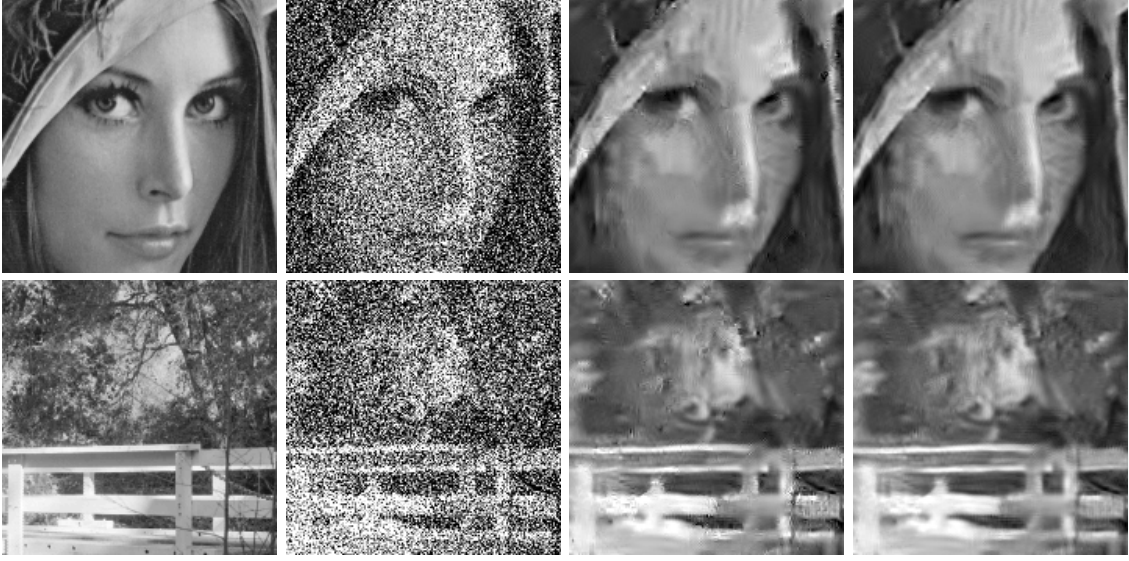


Fig. 1: Results after denoising single-frame datasets with $\sigma_{\text{noise}} = 100$ using BM3D. **Top:** Zoom into the Lena image. **Bottom:** Zoom into the Bridge image. **Left to right:** Original, noisy, single-frame BM3D with and without thresholds.

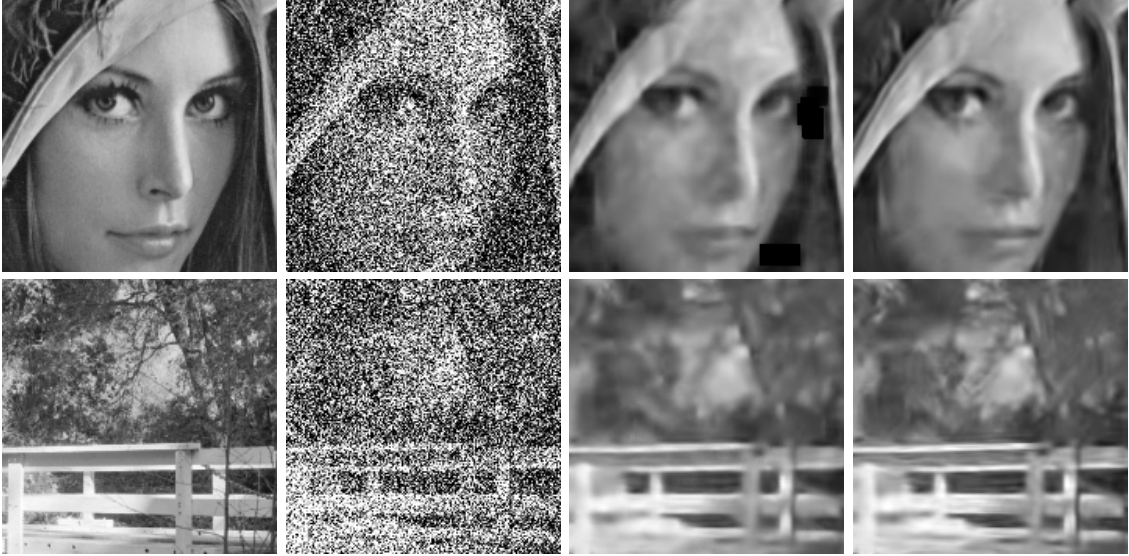


Fig. 2: Results after denoising five-frame datasets with $\sigma_{\text{noise}} = 120$ using BM3D-MF. **Top:** Zoom into the Lena image. **Bottom:** Zoom into the Bridge image. **Left to right:** Original, noisy, BM3D-MF with and without thresholds.

proposed techniques, along with the existing robust optical flow methods employed for registration. In Section III we showcase the results of several denoising experiments. We also give detailed explanations behind the observed ranking of various methods. Finally, in Section IV we conclude our work with a summary and also give a future outlook.

II. MODELING AND THEORY

A. Filters for Single-frame Image Datasets

NLB [18], [19] and BM3D [21], [22] are non-local patch-based denoising methods which consider similar patch information from distant regions in the image. Both single-frame filters are two step methods which combine the denoised image of the initial step with the noisy image in order to derive the

final noise-free image. Furthermore, both of these steps are split into three sub-steps each, namely grouping, collaborative filtering and aggregation.

Grouping: In order to exploit the advantage of having more information, one forms a 3D group of similar patches using L_2 distance, for every noisy reference patch considered.

Collaborative Filtering: The term "collaborative" has a literal meaning here: Each patch in a group collaborates with the rest of the patches for simultaneous and efficient filtering. In NLB, one uses Bayesian filtering (in both main steps) to denoise the 3D groups. In BM3D, a hard thresholding (first main step) and Wiener filtering (second main step) are employed.

Aggregation: In order to derive the final denoised image, one computes a non-linear averaging of the several denoised versions of every pixel.

Image (σ_{noise})	BM-SW	BM-S	BM-MFW	BM-MF
Bridge (80)	391.02	391.72	266.17	266.16
Bridge (100)	463.16	453.37	310.76	307.50
Bridge (120)	1456.35	506.72	434.14	345.19
Peppers (80)	124.08	124.28	59.20	59.20
Peppers (100)	169.10	160.88	74.99	74.15
Peppers (120)	951.5	207.07	335.04	89.64
Lena (80)	143.23	143.78	71.38	71.38
Lena (100)	193.71	183.04	89.85	88.54
Lena (120)	1094.26	238.25	172.57	107.48
House (80)	130.64	132.88	62.60	62.60
House (100)	206.05	187.78	81.52	80.53
House (120)	1213.26	253.73	141.88	96.62

TABLE I: MSE values after denoising using BM3D and BM3D-MF. **Abbreviations:** BM-SW and BM-S stand for single-frame BM3D with and without thresholds, respectively. We have used five-frame datasets for denoising using BM3D-MFW and BM3D-MF.

B. Various Multi-frame Extensions of Single-frame Filters

In this section, we describe the five multi-frame extensions for the above mentioned single-frame filters, in detail. Three of them were introduced in our conference paper [43]. The optimal parameter selections that we introduce for our methods in this paper, will be discussed later on. For a better comprehension, we arrange all the five extensions in an increasing order of complexity in terms of design.

In the multi-frame scenario, there exists slightly different type of data in the temporal and spatial dimensions. Thus, in order to combine them carefully the first two extensions break down spatio-temporal filtering into two stages.

Proposed Extension - AF [43]: First, we average all the frames registered using optical flow. Then we employ a single-frame filter for removing the remaining noise in the averaged frame. *Proposed Extension - FA [43]:* Here, we first denoise every frame by using a single-frame filter and then average the denoised and registered frames.

The above two approaches differ from the methods in [40], [41] in the following fundamental aspect: Irrespective of the quality of registration, we utilise a temporally average and spatially filter strategy. This is different from a temporally average or spatially filter technique that depends on the registration error.

Also, a separable grouping in the temporal and spatial dimensions gives rise to an extra degree of freedom while searching for similar information. The next two approaches exploit this particular advantage by employing a separable spatio-temporal grouping.

Existing Extension - SF [35], [36]: We first consider a single reference frame among all the frames in a dataset and then select reference patches from this frame only. For every reference patch, we consider similar patches from all the frames but not just one frame unlike the single-frame filters.

Proposed Extension - MF [43]: The fourth extension differs from SF in three different steps. Firstly, in order to make complete use of the available information we consider all frames for reference patches. Secondly, we perform an aggregation

of denoised pixels in such a way that after the first main step we have as many denoised frames as there are initial frames. This paves the way for the final difference: For every reference patch we find similar patches from all frames in the second main step also. We cannot do this in the second main step using SF because it has considered reference patches from just one frame. We can thus formulate the aggregation step which yields the final denoised image $\mathbf{u}^{\text{final}}$ from a combination of the noisy image \mathbf{f} and the initial denoised image $\mathbf{u}^{\text{initial}}$, as

$$\mathbf{u}^{\text{final}}(\mathbf{x}) = \frac{\sum_{\ell} \sum_{P_{\ell}} w_{P_{\ell}}^{\text{wien}} \sum_{Q \in P(P_{\ell})} \chi_Q(\mathbf{x}) \mathbf{u}_{Q, P_{\ell}}^{\text{wien}}(\mathbf{x})}{\sum_{\ell} \sum_{P_{\ell}} w_{P_{\ell}}^{\text{wien}} \sum_{Q \in P(P_{\ell})} \chi_Q(\mathbf{x})}. \quad (1)$$

Here, \mathbf{x} denotes the 2D position vector. We represent the set of most similar patches to the reference patch P_{ℓ} belonging to frame ℓ , using $\mathcal{P}(P_{\ell})$. For every patch Q in the set $\mathcal{P}(P_{\ell})$, we have $\chi_Q(\mathbf{x}) = 1$ if $\mathbf{x} \in Q$ and 0 otherwise. The symbol $\mathbf{u}_{Q, P_{\ell}}^{\text{wien}}(\mathbf{x})$ denotes the estimation of the value at pixel position \mathbf{x} , belonging to the patch Q . We derive this estimation through Wiener filtering (with coefficients $w_{P_{\ell}}^{\text{wien}}$) a combination of \mathbf{f} and $\mathbf{u}^{\text{initial}}$. In similar spirit to (1), we can formulate the NLB aggregation process which gives us the final denoised image, as

$$\mathbf{u}^{\text{final}}(\mathbf{x}) = \frac{\sum_{\ell} \sum_{P_{\ell}} \sum_{Q \in P(P_{\ell})} \chi_Q(\mathbf{x}) \mathbf{u}_{Q, P_{\ell}}^{\text{bayes}}(\mathbf{x})}{\sum_{\ell} \sum_{P_{\ell}} \sum_{Q \in P(P_{\ell})} \chi_Q(\mathbf{x})}. \quad (2)$$

Here, the superscript **bayes** implies Bayesian filtering as detailed in [18], [19]. By restricting the total number of frames to one in (1) and (2), we obtain the original single-frame BM3D and NLB algorithms. This implies that MF encompasses the single-frame filters.

While grouping and filtering stages produce noise-free patches, aggregation computes the final denoised image from them. Using a combined spatio-temporal approach gives us an advantage of having more information at the patch denoising steps itself, even before we employ the aggregation process. This exact idea is employed by the final extension.

Existing Extension - CF [37]–[39]: We fix 3D spatio-temporal patches and search for similar volumes instead of patches. We then use a 4D filtering technique that removes noise using all the considered similar volumes. Such ideas are in accordance with the single-frame NLB and BM3D filters, where we employ a 2D similarity measure combined with a 3D denoising technique.

C. Optical Flow Methods Used

As already mentioned, in this work, we perform experiments on both perfectly registered and non-registered datasets. In the latter scenario, we need to first register the images before applying the above multi-frame extensions. Thus, we have employed three robust discontinuity preserving optical flow methods [44]–[46] for this purpose, whose implementations are available in [47]. These motion estimation techniques perform better than some classical strategies [48], [49]. In all the three approaches, we minimise a similar energy functional

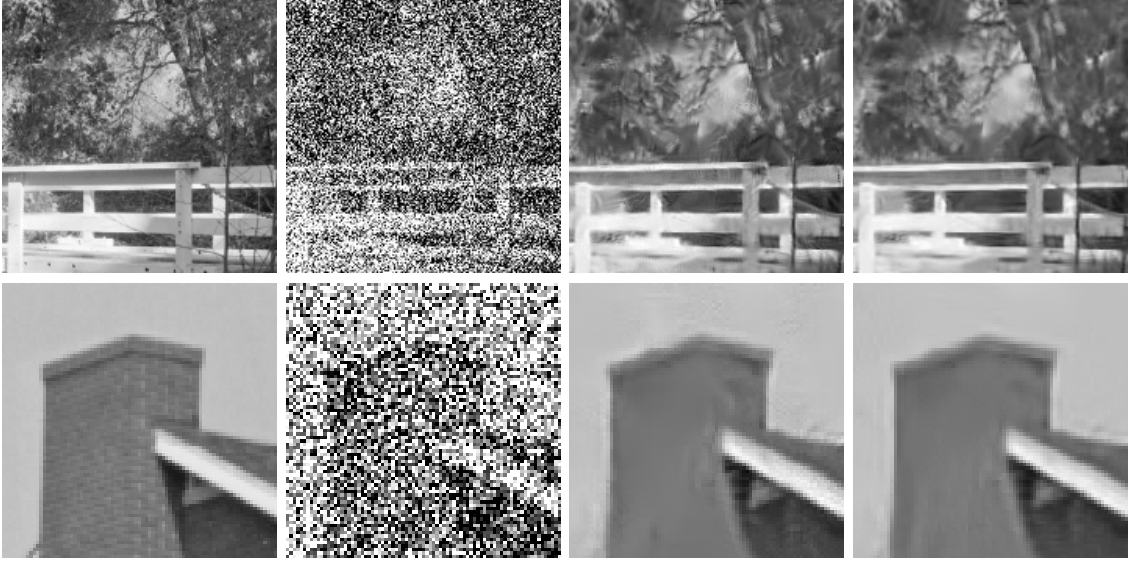


Fig. 3: Results after denoising ten-frame datasets ($\sigma_{\text{noise}} = 120$). **Top:** Zoom into the Bridge image. **Bottom:** Zoom into the House image. **Left to right:** Original, noisy, NLB-AF, BM3D-AF.

Data	NL-AF	NL-FA	NL-SF	NL-MF	NL-CF	BM-AF	BM-MF	BM-CF	NL-AF	NL-FA	NL-SF	NL-MF	NL-CF	BM-AF	BM-MF	BM-CF
B80	211.99	336.31	388.53	339.51	278.02	213.81	266.16	293.64	152.06	325.72	382.08	325.40	237.00	154.42	230.99	277.89
B100	258.57	379.41	433.79	378.04	336.11	254.03	307.50	345.35	186.59	365.85	427.16	362.49	299.14	190.28	268.01	324.65
B120	304.35	410.81	482.66	412.50	388.07	291.80	345.19	391.34	223.20	394.11	472.20	393.75	357.21	223.73	304.76	364.71
P80	55.26	77.19	102.97	72.71	75.91	53.58	59.20	79.57	39.88	70.88	98.79	64.69	62.38	38.68	47.51	71.04
P100	68.76	95.72	130.75	88.68	96.54	67.18	74.15	101.44	47.98	85.20	124.38	77.72	80.07	47.35	58.45	89.68
P120	84.87	113.10	161.67	108.40	119.11	81.99	89.64	124.89	59.13	98.74	152.39	90.86	100.13	57.65	69.91	109.03
L80	63.33	93.85	123.33	94.98	86.09	62.75	71.38	96.68	44.82	87.14	119.61	86.42	69.22	43.79	56.41	83.30
L100	79.39	119.82	157.04	115.52	109.17	77.51	88.54	123.52	55.45	108.27	149.64	103.58	89.88	55.12	70.85	105.73
L120	97.48	136.68	187.06	131.00	133.77	95.42	107.48	151.31	67.93	122.14	175.67	114.81	112.07	66.96	84.99	128.29
H80	57.68	97.00	123.00	78.16	73.17	52.11	62.6	94.50	39.72	85.93	111.67	63.89	56.49	35.53	48.14	83.87
H100	75.06	136.27	161.94	108.74	94.34	67.30	80.53	125.73	49.29	121.68	153.17	87.01	74.88	45.35	63.03	109.06
H120	92.59	176.66	201.99	138.72	119.69	78.81	96.62	159.47	59.93	156.49	191.04	103.32	95.66	53.46	75.15	137.18

TABLE II: MSE values after denoising images with various methods. **Left:** Five-frame datasets. **Right:** Ten-frame datasets. Abbreviations: B80 - Bridge with $\sigma_{\text{noise}} = 80$, P - Peppers, L - Lena, H - Bridge. Sizes: H - 256×256 , rest - 512×512 .

to determine the motion vector $\mathbf{w} = (w_1, w_2, 1)^\top$ from the image sequence f :

$$E(\mathbf{w}) = \int_{\Omega} \left(\Psi(|f(\mathbf{x} + \mathbf{w}) - f(\mathbf{x})|^2) + \gamma (\Psi(|\nabla f(\mathbf{x} + \mathbf{w}) - \nabla f(\mathbf{x})|^2) + \alpha (\Psi(\Phi(\nabla f(\mathbf{x})) \cdot (|\nabla w_1|^2 + |\nabla w_2|^2))) \right) d\mathbf{x}. \quad (3)$$

Here, $\mathbf{x} = (x, y, t)^T$ denotes the spatio-temporal location, Ω is the 2D image domain and ∇ is the spatio-temporal gradient. The above energy penalises deviations in both greyvalues and gradients. We also enable interactions in between neighbouring pixels through the smoothness term. The parameters γ and α represent the gradient and smoothness term weights, respectively. Moreover, we apply $\Psi(s^2) = \sqrt{s^2 + \epsilon^2}$ to attain a robust convex energy functional with $\epsilon = 0.001$ ensuring strict convexity of Ψ . The smoothness function $\Phi(\nabla f, \lambda)$ with parameter λ specifies the regularisation strategy. The three optical flow methods that we use in this work differ in the choice of the function $\Phi(\nabla f, \lambda)$: We will abbreviate these three techniques as SOF-1, SOF-2 and SOF-3. SOF

stands for sub-optimal flow. In SOF-1, we employ a decreasing scalar function [44], [45] for $\Phi(\nabla f, \lambda)$. SOF-2 [46], [47] additionally uses a constant parameter to ensure a minimum isotropic diffusion even when the gradient is very large. In SOF-3 [46], [47], we utilise an automatic selection strategy for λ which helps in dealing with numerical instabilities. We adopt the same minimisation procedure [46], [47] to compute the motion using all the above three methods.

Thus, by combining the five multi-frame extensions and the two single-frame filters, we have ten filters in total. As an example, we will abbreviate one of these combined techniques as BM3D-MF, if it is a combination of single-frame BM3D with extension MF. While we use the above mentioned optical flow strategies for the first four extensions, the fifth method CF (author implementations available in the form of commonly known V-BM4D [38] and V-NLB [39]) uses its own motion compensation techniques. The difference in the various motion estimation approaches used should not be an issue since we are also performing experiments on perfectly registered data.

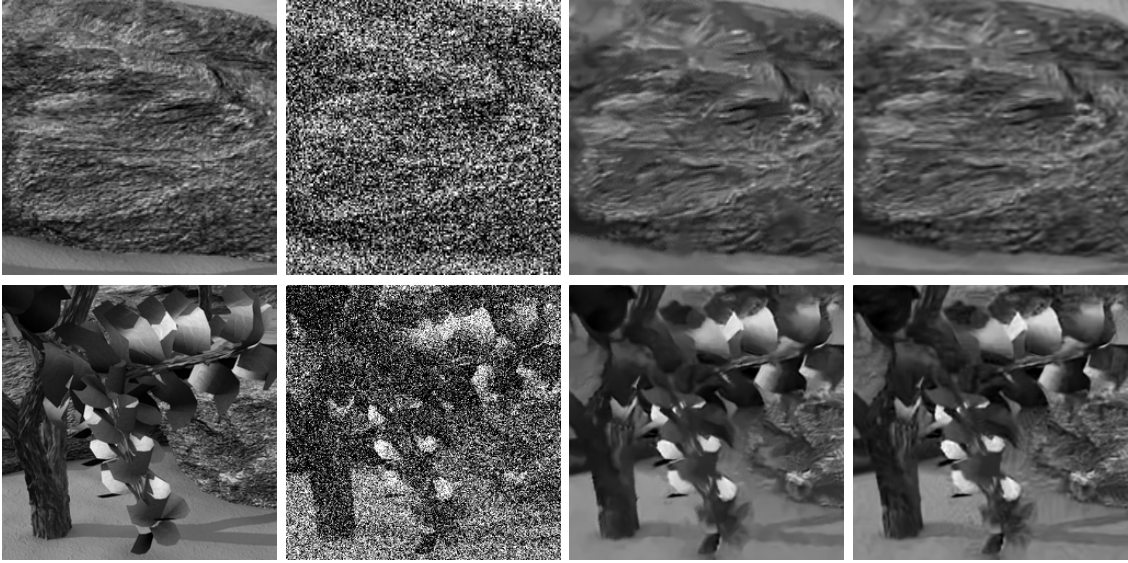


Fig. 4: Results after denoising eight-frame Grove2 dataset with $\sigma_{\text{noise}} = 80$. **Top and bottom:** Zoom into different regions of Grove2 image. **Left to right:** Original, noisy, NLB-AF, BM3D-AF.

Image (σ_{noise})	NLB-AF	NLB-FA	NLB-SF	NLB-MF	NLB-CF	BM-AF	BM-FA	BM-SF	BM-MF	BM-CF
Grove2 (80)	255.76	320.52	352.40	321.57	262.90	236.81	278.37	313.32	268.24	293.62
Grove2 (100)	310.35	353.08	396.51	353.50	313.37	283.65	316.53	364.40	306.47	342.14
Grove2 (120)	344.28	373.29	428.53	373.00	359.31	318.38	344.04	396.27	336.09	384.79
Grove2 (80)	207.29	325.39	353.89	320.46	224.71	206.93	277.36	311.03	251.48	289.51
Grove2 (100)	259.43	347.09	392.41	344.66	276.45	252.05	308.36	360.99	286.07	334.85
Grove2 (120)	308.00	364.70	422.56	364.59	344.50	292.10	334.40	393.68	317.30	373.83

TABLE III: MSE values of denoised Grove2 images after using a combination of denoising methods and optical flow. **Top:** Four-frame datasets (frames 9-12). **Bottom:** Eight-frame datasets (frames 7-14). Frame size: 640×480 .

III. EXPERIMENTS AND DISCUSSION

A. Datasets

For creating perfectly registered data, we have considered multiple AWGN realisations of the classical Lena, House, Peppers and Bridge¹ images with six datasets each (combination of $\sigma_{\text{noise}} = 80, 100, 120$ with five and ten-frame datasets). In a similar spirit, we have also created non-registered data by corrupting the Grove2 [50], Shoe and Bird House [51] images with AWGN.

B. Parameter Selection

Optical Flow Parameters: For the Grove2 dataset, we have optimised the optical flow parameters with respect to the ground truth flow for all three methods. We then choose the best method to register every dataset. For Shoe and Bird House datasets we have optimised the SOF-3 parameters with respect to the final denoised image directly as the ground truth flow was not available. Table IV shows more details.

Denoising Parameters: Various studies [18], [19], [21], [22], [52] have contributed in making the single-frame filters BM3D and NLB parameter selection-free, while retaining the quality of the denoised images as much as possible. In a similar spirit to the above works, in this paper we use better versions of two extensions introduced in our conference paper [43].

Firstly, at the time of application of the filter in the first extension AF, the noise distribution has already changed due to temporal averaging. Since we are using an AWGN model, we know that the standard deviation of noise is reduced by \sqrt{L} times for a dataset with L frames. We can improve the performance of type-AF extensions if we select the filter parameters corresponding to the new standard deviation.

The second improvement is to optimise the number of patches in a 3D group for high amplitude noise elimination using both the original single-frame BM3D filter as well as the BM3D-MF technique. We mentioned in [43] that various extensions of BM3D give better results if we remove the threshold parameters on the L_2 distance during the grouping stage. Here, we show the visual and statistic difference in quality with such a change for both single-frame BM3D and BM3D-MF techniques (Table I and Figures 1 - 2). It is clear that having more patches by removing the thresholds minimises the artifacts in the homogeneous regions and the black square shaped patches in the darker regions of the image are also eliminated. Moreover, in the multi-frame scenario we have more similar patches, when compared to the single-frame layout. We thus check in the upcoming sections, whether an optimised version (BM3D-MFO) of the best performing extension (BM3D-MF) in our conference publication [43], can give even better results by further increasing the number of patches in a 3D group through doubling.

¹<http://sipi.usc.edu/database/>

Image (σ_{noise})	α	γ	λ	AL2E	α	γ	λ	AL2E	α	γ	AL2E	Image (σ_{noise})	α	γ	Image (σ_{noise})	α	γ
Grove2 (80)	45	2.5	0.1	0.612	75	4.5	0.1	0.612	125	1.0	0.640	Shoe(80)	85	0.5	Bird House(80)	130	1.5
Grove2 (100)	35	2.0	0.1	0.669	15	0.5	0.1	0.667	110	1.0	0.632	Shoe(100)	95	0.5	Bird House(100)	100	1.5
Grove2 (120)	20	1.0	0.1	0.742	20	1.0	0.1	0.742	95	1.0	0.711	Shoe(120)	90	0.5	Bird House(120)	90	1.5

TABLE IV: Optical flow parameter values used for different datasets along with average L_2 error (AL2E). **Left, Centre-left, Centre:** Grove2 dataset with SOF-1, SOF-2 and SOF-3 methods, respectively. We have considered the tenth frame as the reference frame since ground truth flow information was available between frames 10 and 11. **Centre-Right:** Shoe dataset with SOF-3 method. **Right:** Bird House dataset with SOF-3 method. We have utilised the fifth frame as the reference frame for both these datasets and then employed frames 4-6 for optimising the optical flow parameters. Also, we have used BM3D-MF and BM3D-FA as denoising methods for optimising SOF parameters for these two datasets, respectively.

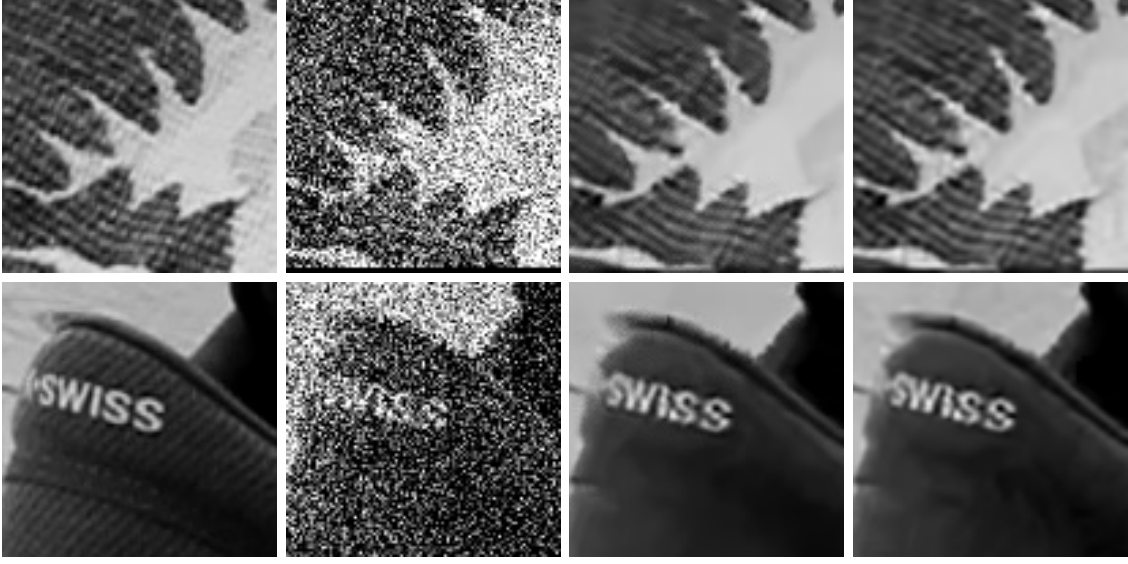


Fig. 5: Results after denoising ten-frame Shoe dataset ($\sigma_{\text{noise}} = 80$). **Top and bottom:** Zoom into different regions of Shoe image. **Left to right:** Original, noisy, NLB-AF, BM3D-AF.

Image (σ_{noise})	NLB-AF	NLB-FA	NLB-SF	NLB-MF	NLB-CF	BM-AF	BM-FA	BM-SF	BM-MF	BM-MFO	BM-CF
Shoe (80)	80.51	116.79	141.01	111.44	91.35	70.49	87.46	113.21	81.00	80.66	102.88
Shoe (100)	96.86	135.86	168.07	127.23	115.11	84.14	105.91	140.53	100.91	97.16	131.39
Shoe (120)	112.71	150.84	193.62	141.00	139.17	99.79	124.48	167.11	119.82	115.49	160.30
Shoe (80)	63.15	114.15	137.40	102.70	81.59	56.42	80.74	109.04	68.42	66.54	91.15
Shoe (100)	75.67	129.50	164.13	115.89	102.54	66.01	96.83	134.21	84.43	79.76	113.83
Shoe (120)	88.08	140.24	188.83	126.65	124.22	76.87	111.64	161.66	102.79	95.01	136.89

TABLE V: MSE values of denoised Shoe images after using a combination of denoising methods and optical flow. **Top:** Five-frame datasets (frames 3-7). **Bottom:** Ten-frame datasets (frames 1-10). Frame size: 1280×720 . **Abbreviation:** BM-MFO uses twice the number of patches as in BM-MF.

For the denoised results of perfectly registered noisy data using SF and CF extensions, we have always presented the best MSE value among all frames. For experiments on non-registered datasets, we have calculated the MSE value by leaving out a border of fifty pixels on all sides of the reference frame at which different frames were registered. We do this in order to mitigate the ill-effects due to unavailable information at the borders of registered images. This also makes sense in multi-frame imaging because we capture the region of interest in the centre of the frame.

C. Perfectly Registered Datasets

Table II showcases the MSE values of the denoised images and Figure 3 displays the visual results, after we have applied

all ten methods. It is clear from these results that extensions of type-AF outperform all other techniques. They are superior to type-MF methods (which is in contradiction to our conference paper) as we account for the change in the noise distribution due to temporal averaging.

In the category-FA extensions, we directly apply the single-frame filters on every frame. This is a sub-optimal solution because we do not have enough signal on each of the frames. Techniques belonging to type-SF do not make use of the complete available information as they just consider a single reference frame.

In the MF and CF filters, we avoid the disadvantages of both FA and SF. However, they fall behind type-AF methods for two reasons: Firstly, we separate out temporal and spatial

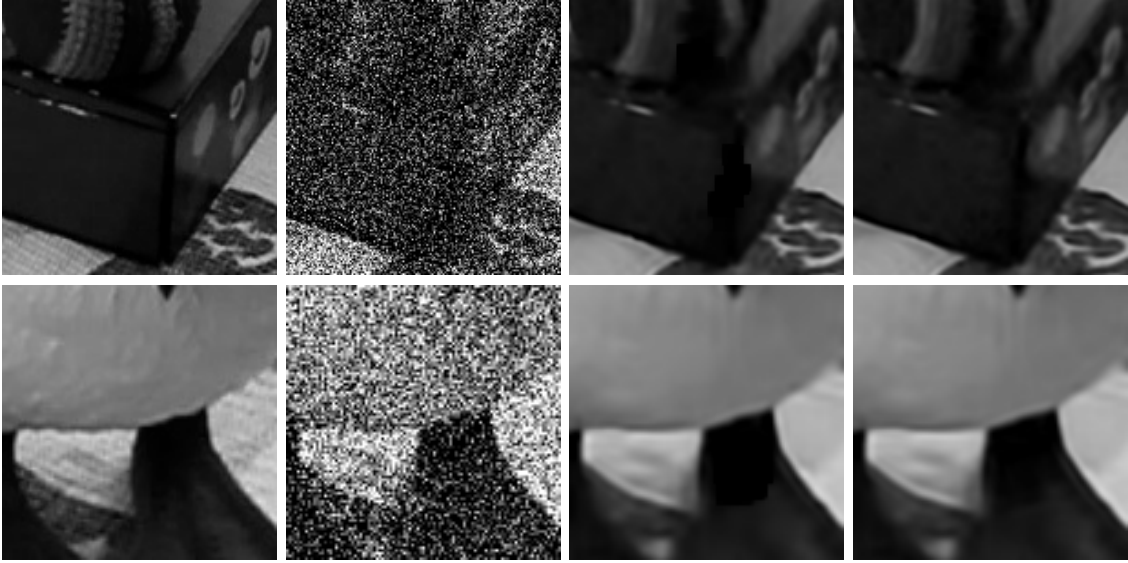


Fig. 6: Results after denoising ten-frame Shoe dataset with $\sigma_{\text{noise}} = 80$. **Top and bottom:** Zoom into different regions of Shoe image. **Left to right:** Original, noisy, BM3D-MF, BM3D-MFO (twice the number of patches than normal).

filtering in category-AF techniques. This is advantageous since we have noisy versions of the same original greyvalue in the temporal dimension for perfectly registered images. In the spatial dimensions we have noisy versions of approximately equal grey values in general. This outperforms simultaneous non-linear filtering of the final two types of techniques, where we combine the information in all dimensions at one go. Such a strategy proves to be inferior even though we use a non-linear filtering in the temporal dimension when compared to the linear temporal averaging of category-AF filters. This is because linear averaging of different noisy versions of the same pixel intensity does not create artifacts like combination with dissimilar pixel intensities does. This is in congruence with why averaging is preferred in electron microscopy (Chapter 11 of [53]). Moreover, the linear averaging helps in computing the new standard deviation of noise after temporal averaging through theoretical knowledge. Secondly, BM3D-AF and NLB-AF compute the grouping on the less noisy averaged image. In all the other four categories we do this on the highly noisy initial images, which makes the grouping error-prone.

The final remaining comparison is between MF and CF techniques: We can attribute the superior performance of BM3D-MF, when compared to present state-of-the-art NLB-CF and BM3D-CF methods, to the extra degree of freedom in the similarity measure during the grouping stage.

The overall better performance of type-AF filters does not mean we can immediately reject the next best MF and CF categories. We must remember that we assumed AWGN noise and perfect registration. In the first scenario, we were able to optimise the denoising ability of NLB-AF and BM3D-AF easily for AWGN. This is because of its signal independent nature, which helped in proper selection of filtering parameters through theoretical knowledge of the change in noise distribution due to temporal averaging. For noise of Poissonian type for example, AWGN elimination methods are normally

combined with variance stabilising transformations (VST) for noise elimination. This combination with VSTs and noise of signal dependent nature makes it difficult to optimise for the change in noise distribution. In another recent paper [54], we evaluated the first four BM3D extensions in the Poissonian noise scenario and observed similar results as for our Gaussian noise study [43]: BM3D-MF outperformed BM3D-AF. This is because we cannot straightforwardly compute the new standard deviation of noise after temporal averaging in the Poissonian noise scenario. We speculate that employing a more sophisticated VST framework (see eg. [55], [56]) could help in accounting for the imprecision in variable stabilisation for all extensions. Furthermore, it might help in dealing with the additional imprecision caused due to change in the noise distribution in AF techniques. The second scenario where we cannot reject methods from categories other than type-AF is for imperfect registrations. We will examine this situation in the upcoming section where we consider non-registered datasets.

Furthermore, BM3D-AF is superior to NLB-AF (from Table II and Figure 3) because BM3D is a better single-frame denoising method than NLB for greyvalue images. Even though both NLB and BM3D use Wiener filtering, BM3D additionally uses the discrete cosine transform (DCT) and the bi-orthogonal spline wavelet transform (BIOR) in the two main steps, respectively. We infer that the directional information preserved by the DCT and BIOR transforms leads to the superior edge-preservation of BM3D when compared to NLB.

D. Non-registered Datasets

Tables III, V and VI display the MSE values of the denoised images while Figures 4, 5 and 7 showcase the visual results. It can be clearly seen that NLB-AF and BM3D-AF are also significantly better for non-registered datasets. The superior registration capabilities of the robust optical flow methods and

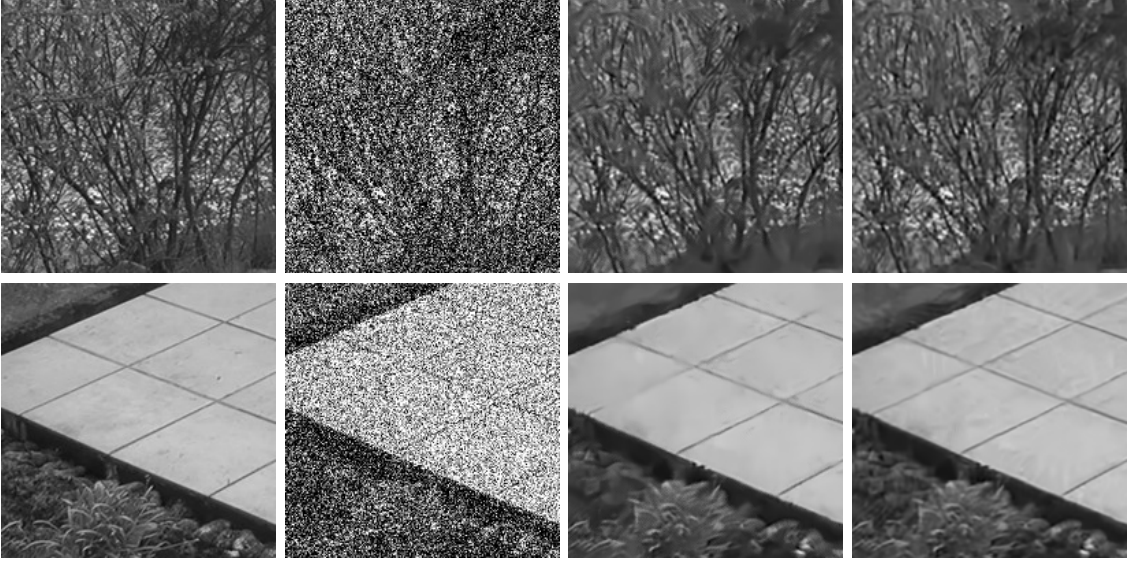


Fig. 7: Results after denoising ten-frame Bird House dataset ($\sigma_{\text{noise}} = 80$). **Top to bottom:** Zoom into different regions of Bird House image. **Left to right:** Original, noisy, NLB-AF, BM3D-AF.

Image (σ_{noise})	NLB-AF	NLB-FA	NLB-SF	NLB-MF	NLB-CF	BM-AF	BM-FA	BM-SF	BM-MF	BM-CF
Bird House (80)	138.67	230.59	255.74	237.26	190.15	131.30	182.07	211.31	167.51	210.40
Bird House (100)	173.86	248.54	275.76	251.22	224.40	162.35	207.03	242.42	194.50	247.52
Bird House (120)	207.70	261.07	295.32	262.32	254.40	193.34	227.89	269.64	217.17	279.67
Bird House (80)	107.85	230.77	252.51	233.67	183.59	105.29	187.48	206.18	148.34	203.06
Bird House (100)	138.77	242.64	270.78	244.28	218.01	134.66	220.37	236.66	172.51	236.73
Bird House (120)	168.58	251.84	288.16	254.41	247.59	166.80	222.61	261.38	194.95	264.05

TABLE VI: MSE values of denoised Bird House images after using a combination of denoising methods and optical flow. **Top:** Five-frame datasets (frames 3-7). **Bottom:** Ten-frame datasets (frames 1-10). Frame size: 1280×720 .

the previously mentioned modelling advantages of type-AF techniques are the main reasons behind this. Moreover, we speculate that the final 2D spatial filtering operation after the temporal averaging in NLB-AF and BM3D-AF, also inherently accounts for the misregistered pixels.

The BM3D-MFO variant helps in removing black patches in darker regions of the image. The decrease in MSE values from BM3D-MF to BM3D-MFO in Table V indicates that the black patches are eliminated by doubling the number of patches (Figure 6). However, we must use the above strategy of increasing the number of patches only if we encounter black patches. Having too many patches in a 3D group would instead give rise to an undesirable blurring.

We can thus infer two conclusions from our results: The latest robust optical flow methods are also capable of preserving the best performing nature of average-filter (AF) multi-frame filters in the non-registered datasets scenario. Secondly, in the future we should concentrate on methods which separate the filtering in spatial and temporal dimensions for ideal as well as practical situations, like BM3D-AF and NLB-AF.

All the above results show that type-AF filters are the superior methods irrespective of whether there is any motion or not in the image dataset, what criteria have been used to optimise the optical flow, and what kind of optical flow method has been employed. For future references, we abbreviate BM3D-AF as BM3D-OF (3D block matching combined with

optical flow) as it represents the new state-of-the-art standard in multi-frame image denoising.

In future, BM3D-OF can be combined with occlusion handling techniques in [42] as well as deflickering and sharpening strategies in [38], for further qualitative improvement. We can also consider replacing BM3D with better single-frame filters and the present optical flow methods with even better motion estimation algorithms, for state-of-the-art results.

E. Computational Time

The BM3D-OF framework is the fastest among all extensions as it employs separable spatio-temporal filtering: Temporal averaging can be performed in real time. Thus, the net complexity is just a combination of the optical flow method and the 2D single-frame filter employed on the temporally averaged frame. To elaborate further, let us consider BM3D-MF which is the next best extension after the first category techniques. Our experimental demonstrations on an Intel(R) Core(TM) i7-6700 CPU @3.4 GHz using C++ and OpenMP, were eleven times slower for BM3D-MF when compared to the original single channel BM3D (5-frame 256×256 sized House dataset). This factor is slightly more than twice the number of frames that we used. It can be attributed to considering every frame as the reference frame instead of just one as well as to the extensive patch-search across all frames. We also have a GPU implementation of BM3D-MF using ANSI C and

CUDA which takes 2.7 seconds on an NVIDIA Quadro P5000 architecture. This was about 6.5 times faster than the parallel CPU implementation. We have already shown that BM3D-MF encompasses BM3D-OF mathematically. Thus, the same GPU implementation can also be employed for BM3D-OF by just changing the number of frames to one and using the new standard deviation of noise after temporal averaging, as input.

IV. CONCLUSIONS AND OUTLOOK

We have optimised the usage of NLB and BM3D filters for the multi-frame scenario by proposing two novel extensions and evaluating them with three other possible approaches. We can conclude from the experiments that our proposed sequential process of registering the images with robust optical flow methods, temporally averaging the registered noisy images, and then applying the single-frame filters with optimal parameters corresponding to the new noise distribution after temporal averaging, gives the best results. This is true for both NLB and BM3D, an observation which has surprisingly not been recognised for many years. This re-affirms the fact that sometimes the simpler methods are the most powerful ones. Furthermore, the significant quality improvement comes with zero additional parameters and less computational costs. The technique preserves a large amount of detail even when the images are corrupted with noise of very high amplitude. BM3F-OF is also robust with respect to several factors related to optical flow computation and thus can be employed in practice for many other multi-frame image processing applications.

Combining BM3D-OF with variance stabilising transformations, deflickering, sharpening and occlusion handling techniques will be considered in our future research. We will also use BM3D-OF as a regulariser in PDEs for robust multi-frame image reconstruction applications [57]–[60].

Acknowledgements. J.W. has received funding from the European Research Council (ERC) under the European Union’s Horizon 2020 research and innovation programme (grant no. 741215, ERC Advanced Grant INCOVID).

We thank Prof. Karen Egiazarian from Tampere University, Finland. A valuable discussion with him has helped to improve the evaluation part of this work. We also thank our colleagues Dr. Matthias Augustin and Dr. Pascal Peter for useful comments on a draft version of the paper.

REFERENCES

- [1] T. Huang, *Advances in Computer Vision and Image Processing*. Greenwich, CT: JAI Press, 1986.
- [2] L. Shapiro and G. Stockman, *Computer Vision*. Englewood Cliffs, NJ: Prentice-Hall, 2001.
- [3] B. Keelan and R. Cookingham, *Handbook of Image Quality*. Boca Raton, FL: CRC Press, 2002.
- [4] F. Rooms, W. Philips, and P. V. Oostveldt, “Integrated approach for estimation and restoration of photon-limited images based on steerable pyramids,” in *Proc. 2003 IEEE EURASIP Conference Focussed on Video/Image Processing and Multimedia Communications*, Zagreb, Croatia, Jul. 2003, pp. 131–136.
- [5] R. Gonzalez and R. Woods, *Digital Image Processing*. Englewood Cliffs, NJ: Prentice-Hall, 2007.
- [6] I. Rodrigues, J. Sanches, and J. Bioucas-Dias, “Denoising of medical images corrupted by Poisson noise,” in *Proc. 2008 IEEE International Conference on Image Processing*, San Diego, CA, USA, Oct. 2008, pp. 1756–1759.
- [7] J. Jinschek, K. Batenburg, H. Calderon, R. Kilaas, V. Radmilovic, and C. Kisielowski, “3D reconstruction of the atomic positions in a simulated gold nanocrystal based on discrete tomography: Prospects of atomic resolution electron tomography,” *Ultramicroscopy*, vol. 108, no. 6, pp. 589–604, May 2008.
- [8] C. Bonchelet, *Image Noise Models*, 2nd ed., ser. The Essential Guide to Image Processing, A. Bovik, Ed. New York: Academic Press, Jul. 2009, pp. 143–167.
- [9] L. Azzari, L. Borges, and A. Foi, *Modeling and Estimation of Signal-Dependent and Correlated Noise*, ser. Denoising of Photographic Images and Video: Fundamentals, Open Challenges and New Trends, M. Bertalmio, Ed. Switzerland: Springer, 2018, pp. 1–36.
- [10] F. J. Anscombe, “The transformation of Poisson, binomial and negative-binomial data,” *Biometrika*, vol. 35, no. 3/4, pp. 246–254, Dec. 1948.
- [11] M. Mäkitalo and A. Foi, “Optimal inversion of the Anscombe transformation in low-count Poisson image denoising,” *IEEE Transactions on Image Processing*, vol. 20, no. 1, pp. 99–109, Jan. 2011.
- [12] —, “Optimal inversion of the generalized Anscombe transformation for Poisson-Gaussian noise,” *IEEE Transactions on Image Processing*, vol. 22, no. 1, pp. 91–103, Jan. 2013.
- [13] J. Weickert, “Theoretical foundations of anisotropic diffusion in image processing,” in *Theoretical Foundations of Computer Vision*, ser. Computing Supplement, W. Kropatsch, R. Klette, F. Solina, and R. Albrecht, Eds. Vienna: Springer, 1996, vol. 11, pp. 221–236.
- [14] —, “Coherence-enhancing diffusion filtering,” *International Journal of Computer Vision*, vol. 31, no. 2/3, pp. 111–127, Apr. 1999.
- [15] B. Maiseli, N. Ally, and H. Gao, “A noise-suppressing and edge-preserving multiframe super-resolution image reconstruction method,” *Signal Processing: Image Communication*, vol. 34, pp. 1–13, May 2015.
- [16] I. Mourabit, M. Rhabi, A. Hakim, A. Laghrib, and E. Moreau, “A new denoising model for multi-frame super-resolution image reconstruction,” *Signal Processing*, vol. 132, pp. 51–65, Mar. 2017.
- [17] W. Richardson, “Bayesian-based iterative method of image restoration,” *Journal of the Optical Society of America A*, vol. 62, no. 1, pp. 55–69, Jan. 1972.
- [18] M. Lebrun, A. Buades, and J. Morel, “A nonlocal Bayesian image denoising algorithm,” *SIAM Journal on Imaging Sciences*, vol. 6, no. 3, pp. 1665–1688, Sep. 2013.
- [19] —, “Implementation of the non-local Bayes (NL-Bayes) image denoising algorithm,” *Image Processing On Line*, vol. 3, pp. 1–42, Jun. 2013.
- [20] L. Yaroslavsky and M. Eden, *Fundamentals of Digital Optics: Digital Signal Processing in Optics and Holography*, 1st ed. Berlin: Springer, 1996.
- [21] K. Dabov, A. Foi, V. Katkovnik, and K. Egiazarian, “Image denoising by sparse 3-d transform-domain collaborative filtering,” *IEEE Transactions on image processing*, vol. 16, no. 8, pp. 2080–2095, Aug. 2007.
- [22] M. Lebrun, “An analysis and implementation of the BM3D image denoising method,” *Image Processing On Line*, vol. 2, pp. 175–213, Aug. 2012.
- [23] A. Buades, B. Coll, and J. Morel, “A non-local algorithm for image denoising,” in *Proc. 2005 IEEE Computer Society Conference on Computer Vision and Pattern Recognition*, vol. 2, San Diego, CA, Jun. 2005, pp. 60–65.
- [24] A. Buades, B. Coll, and J.-M. Morel, “A review of image denoising algorithms, with a new one,” *Multiscale Modeling and Simulation*, vol. 4, no. 2, pp. 490–530, 2005.
- [25] C. Cruz, A. Foi, V. Katkovnik, and K. Egiazarian, “Nonlocality-reinforced convolutional neural networks for image denoising,” *IEEE Signal Processing Letters*, vol. 25, no. 8, pp. 1216–1220, Aug. 2018.
- [26] F. Luisier, C. Vonesch, T. Blu, and M. Unser, “Fast Haar-wavelet denoising of multidimensional fluorescence microscopy data,” in *Proc. 2009 IEEE International Symposium on Biomedical Imaging: From Nano to Macro*, Boston, MA, USA, Jul. 2009, pp. 310–313.
- [27] S. Delpretti, F. Luisier, S. Ramani, T. Blu, and M. Unser, “Multiframe SURE-LET denoising of timelapse fluorescence microscopy images,” in *Proc. 2008 IEEE International Symposium on Biomedical Imaging: From Nano to Macro*, Paris, France, May 2008, pp. 149–152.
- [28] A. M. Hasan, A. Melli, K. A. Wahid, and P. Babyn, “Denoising low-dose CT images using multi-frame blind source separation and block matching filter,” *IEEE Transactions on Radiation and Plasma Medical Sciences*, vol. 2, no. 4, pp. 279–287, Jul. 2018.
- [29] J. Boulanger, C. Kervrann, P. Bouthemy, P. Elbau, J. B. Sibarita, and J. Salamero, “Patch-based nonlocal functional for denoising fluorescence microscopy image sequences,” *IEEE Transactions on Medical Imaging*, vol. 29, no. 2, pp. 442–454, Feb. 2010.

- [30] W. Dong, T. Huang, G. Shi, Y. Ma, and X. Li, "Robust tensor approximation with Laplacian scale mixture modeling for multiframe image and video denoising," *IEEE Journal of Selected Topics in Signal Processing*, vol. 12, no. 6, pp. 1435–1448, Oct. 2018.
- [31] R. Hao and Z. Su, "A patch-based low-rank tensor approximation model for multiframe image denoising," *Journal of Computational and Applied Mathematics*, vol. 329, pp. 125–133, Feb. 2018.
- [32] L. Fang, S. Li, Q. Nie, J. A. Izatt, C. A. Toth, and S. Farsiu, "Sparsity based denoising of spectral domain optical coherence tomography images," *Biomedical Optics Express*, vol. 3, no. 5, pp. 927–942, 2012.
- [33] E. Gil-Rodrigo, J. Portilla, D. Miraut, and R. Suarez-Mesa, "Efficient joint Poisson-Gauss restoration using multi-frame L2-relaxed-L0 analysis-based sparsity," in *Proc. 2011 IEEE International Conference on Image Processing*, Brussels, Belgium, Sep. 2011, pp. 1385–1388.
- [34] L. Zhang, S. Vaddadi, H. Jin, and S. K. Nayar, "Multiple view image denoising," in *Proc. 2009 IEEE Conference on Computer Vision and Pattern Recognition*, Miami, FL, USA, Jun. 2009, pp. 1542–1549.
- [35] A. Buades, B. Coll, and J. Morel, "Denoising image sequences does not require motion estimation," in *Proc. 2005 IEEE Conference on Advanced Video and Signal Based Surveillance*, Como, Italy, Sep. 2005, pp. 70–74.
- [36] M. Tico, "Multi-frame image denoising and stabilization," in *Proc. 2008 IEEE European Signal Processing Conference*, Lausanne, Switzerland, Aug. 2008, pp. 1–4.
- [37] M. Maggioni, V. Katkovnik, K. Egiazarian, and A. Foi, "Nonlocal transform-domain filter for volumetric data denoising and reconstruction," *IEEE Transactions on Image Processing*, vol. 22, no. 1, pp. 119–133, Jan. 2013.
- [38] M. Maggioni, G. Boracchi, A. Foi, and K. Egiazarian, "Video denoising, deblocking, and enhancement through separable 4-d nonlocal spatiotemporal transforms," *IEEE Transactions on Image Processing*, vol. 21, no. 9, pp. 3952–3966, Sep. 2012.
- [39] P. Arias and J. M. Morel, "Video denoising via empirical Bayesian estimation of space-time patches," *Journal of Mathematical Imaging and Vision*, vol. 60, no. 1, pp. 70–93, Jan. 2018.
- [40] T. Buades, Y. Lou, J. M. Morel, and Z. Tang, "A note on multi-image denoising," in *Proc. 2009 IEEE International Workshop on Local and Non-Local Approximation in Image Processing*, Tuusula, Finland, Oct. 2009, pp. 1–15.
- [41] A. Buades, Y. Lou, J. M. Morel, and Z. Tang, "Multi Image Noise Estimation and Denoising," *HAL Archives*, hal-00510866, version 1, Aug. 2010.
- [42] A. Buades, J. L. Lisani, and M. Miladinović, "Patch-based video denoising with optical flow estimation," *IEEE Transactions on Image Processing*, vol. 25, no. 6, pp. 2573–2586, Jun. 2016.
- [43] K. Bodduna and J. Weickert, "Enhancing patch-based methods with inter-frame connectivity for denoising multi-frame images," in *Proc. 2019 IEEE International Conference on Image Processing*, Taipei, Taiwan, Sep. 2019, pp. 2414–2418.
- [44] L. Alvarez, M. Esclarin, M. Lefebvre, and J. Sanchez, "A PDE model for computing the optical flow," in *Proc. XVI Congreso de Ecuaciones Diferenciales y Aplicaciones*, Las Palmas de Gran Canaria, Spain, Sep. 1999, pp. 1349–1356.
- [45] J. Revaud, P. Weinzaepfel, Z. Harchaoui, and C. Schmid, "Epicflow: Edge-preserving interpolation of correspondences for optical flow," in *Proc. 2015 IEEE Conference on Computer Vision and Pattern Recognition*, Boston, Massachusetts, Jun. 2015, pp. 1164–1172.
- [46] N. Monzon, A. Salgado, and J. Sanchez, "Regularization strategies for discontinuity-preserving optical flow methods," *IEEE Transactions on Image Processing*, vol. 25, no. 4, pp. 1580–1591, Apr. 2016.
- [47] —, "Robust discontinuity preserving optical flow methods," *Image Processing On Line*, vol. 6, pp. 165–182, Nov. 2016.
- [48] T. Brox, A. Bruhn, N. Papenberger, and J. Weickert, "High accuracy optical flow estimation based on a theory for warping," in *Computer Vision – ECCV 2004, Part IV*, ser. Lecture Notes in Computer Science, T. Pajdla and J. Matas, Eds. Berlin: Springer, 2004, vol. 3024, pp. 25–36.
- [49] C. Zach, T. Pock, and H. Bischof, "A duality based approach for realtime TV-L1 optical flow," in *Pattern Recognition, DAGM 2007*, ser. Lecture Notes in Computer Science, F. A. Hamprecht, C. Schnörr, and B. Jähne, Eds., vol. 4713. Berlin: Springer, 2007, pp. 214–223.
- [50] S. Baker, D. Scharstein, J. Lewis, S. Roth, M. J. Black, and R. Szeliski, "A database and evaluation methodology for optical flow," *International Journal of Computer Vision*, vol. 92, no. 1, pp. 1–31, Nov. 2010.
- [51] B. Ummenhofer and T. Brox, "Dense 3D reconstruction with a hand-held camera," in *Pattern Recognition, DAGM/OAGM 2012*, ser. Lecture Notes in Computer Science, A. Pinz, T. Pock, H. Bischof, and F. Leberl, Eds., vol. 7476. Graz, Austria: Springer, 2012, pp. 103–112.
- [52] Y. Hou, C. Zhao, D. Yang, and Y. Cheng, "Comments on 'Image denoising by sparse 3-D transform-domain collaborative filtering,'" *IEEE Transactions on Image Processing*, vol. 20, no. 1, pp. 268–270, Jan. 2011.
- [53] J. Frank, *Electron Tomography: Methods for Three-dimensional Visualization for Structures in the Cell*, 2nd ed. New York: Springer, 2008.
- [54] K. Bodduna and J. Weickert, "Poisson noise removal using multi-frame 3D block matching," in *Proc. IEEE European Workshop on Visual Information Processing*, Rome, Italy, Oct. 2019, pp. 58–63.
- [55] M. Mäkitalo and A. Foi, "A closed-form approximation of the exact unbiased inverse of the Anscombe variance-stabilizing transformation," *IEEE Transactions on Image Processing*, vol. 20, no. 9, pp. 2697–2698, Sep. 2011.
- [56] L. Azzari and A. Foi, "Variance stabilization for noisy+estimate combination in iterative Poisson denoising," *IEEE Signal Processing Letters*, vol. 23, no. 8, pp. 1086–1090, Aug. 2016.
- [57] A. Buades, J. Duran, and J. Navarro, "Motion-compensated spatiotemporal filtering for multi-image and multimodal super-resolution," *International Journal of Computer Vision*, vol. 127, no. 10, pp. 1474–1500, Oct. 2019.
- [58] A. Buades and J. L. Lisani, "Enhancement of noisy and compressed videos by optical flow and non-local denoising," *IEEE Transactions on Circuits, Systems and Video Technology*, Apr. 2019, Early Access.
- [59] K. Bodduna and J. Weickert, "Evaluating data terms for variational multi-frame super-resolution," in *Scale Space and Variational Methods in Computer Vision*, ser. Lecture Notes in Computer Science, F. Lauze, Y. Dong, and A. Dahl, Eds., vol. 10302. Berlin: Springer, 2017, pp. 590–601.
- [60] K. Bodduna, J. Weickert, and A. S. Frangakis, "Hough based evolutions for enhancing structures in 3D electron microscopy," in *Computer Analysis of Images and Patterns (CAIP)*, ser. Lecture Notes in Computer Science, M. Vento and G. Percannella, Eds., vol. 11678. Springer, Cham, 2019, pp. 102–112.



Kireeti Bodduna received his Bachelor and Master degrees in Physics from the Indian Institute of Science Education and Research (Kolkata, India), in 2014. He then completed graduate level coursework in the Saarbrücken Graduate School of Computer Science and is now a Ph.D. student at the Mathematical Image Analysis Group, Saarland University (Saarbrücken, Germany). He is interested in designing robust methods for recovering digital images in the presence of various noise distributions using diffusion and patch-based techniques.



Joachim Weickert is a Professor of Mathematics and Computer Science at Saarland University (Saarbrücken, Germany), where he heads the Mathematical Image Analysis Group. He graduated and obtained his Ph.D. from the University of Kaiserslautern (Germany) in 1991 and 1996. He worked as post-doctoral researcher at the University Hospital of Utrecht (The Netherlands) and the University of Copenhagen (Denmark), and as assistant professor at the University of Mannheim (Germany). Joachim Weickert has developed many models and efficient algorithms for image processing and computer vision using partial differential equations and variational methods. He is Editor-in-Chief of the Journal of Mathematical Imaging and Vision.